JOURNAL OF MATERIALS SCIENCE 32 (1997) 503–511

Alumina–mullite–zirconia composites

Part II *Microstructural development and toughening*

H. M. JANG*, S. M. CHO, K. T. KIM‡
Department of Materials Science and Engineering, and ‡Department of Mechanical Engineering, Pohang University of Science and Technology (POSTECH), Pohang 790-784, Republic of Korea

Densification characteristics and fracture toughness of the alumina–mullite–zirconia (AMZ) composites fabricated by the colloidal mixing route were examined. The densification of boehmite–silica–zirconia precursor compacts was characterized by three distinct stages. Stage I was represented by a rapid shrinkage between 1100 and 1300 °C and was caused by the viscous flow sintering of the SiO_2 component. Stage II was characterized by a temporary cessation of the shrinkage caused by the mullitization. Stage III was represented by a restoration of the shrinkage for temperatures above 1450 °C. The α-Al_2O_3 seeding facilitated the formation of elongated grains in the AMZ composites, and these elongated grains correspond to α-Al_2O_3. The toughening caused by the microcrack nucleation was comparable to that by the t → m martensitic transformation and increased with increasing total content of zirconia.

1. Introduction

In a previous paper [1], we proposed and tested a new colloidal processing scheme for fabricating dense alumina–mullite–zirconia (AMZ) composite with a uniform microstructure. We also systematically investigated the phase-formation characteristics of boehmite–silica–zirconia precursor system and found that the sequences of solid-state reactions occurring in the precursor powders were greatly influenced by the α-Al_2O_3 seedling.

In the present work, we systematically examined densification characteristics and microstructural development of the AMZ composites prepared by the colloidal processing route discussed in the previous paper [1]. Using a semi-empirical relationship between the increment in the fracture toughness and the total zirconia content, we have also estimated separately the relative contributions of the tetragonal → monoclinic transformation and the microcrack nucleation to the net toughening increment.

2. Experimental procedure

Detailed experimental descriptions of the fabrication of AMZ composites and the measurement of colloid/interface variables relevant to the present study were given in the previous paper [1]. Unless specified elsewhere, the composition of AMZ composites used in this study was 50 wt % alumina–30 wt % mullite–20 wt % zirconia (after sintering).

The cold isostatically pressed pellets were sintered in air at various temperatures below 1600 °C for 1 h with both heating and cooling rates of 5 °C min^{-1}. Sintered compacts were analysed for phase identity using an X-ray diffractometer (DMAX-3B, Rigaku, Japan). The bulk densities of sintered specimens were determined by the modified Archimedes method (ASTM C-20), and the relative densities (% theoretical density) were then calculated from the starting compositions and the phase information provided using XRD analysis. The microstructural analysis of the sintered specimen was done using a scanning electron microscope (S-570, Hitachi, Tokyo, Japan). The microchemical feature of composite specimens was examined by EPMA point analysis and elemental silicon-mapping (Jeol, JXA-733, Japan).

The fracture toughness values of sintered composites were determined using an indentation-fracture method. Vickers diamond pyramid indentations (Dia Tester 2RC, Amsler Otto Wolpert-Werke, GmbH, Germany) were then made on the polished specimens using a 5 kg indentation load. The holding time after an indent was 10 s. Data were obtained using at least five indentations on each specimen. The critical stress intensity factor, K_{1c}, was then estimated using the crack length and the analysis described by Lawn and Fuller [2].

3. Results and discussion

3.1. Densification characteristics

The relative density of both α-Al_2O_3 seeded and unseeded composite specimens increases rapidly with increasing sintering temperature (Fig. 1). The α-Al_2O_3

*Author to whom all correspondence should be addressed.

0022–2461

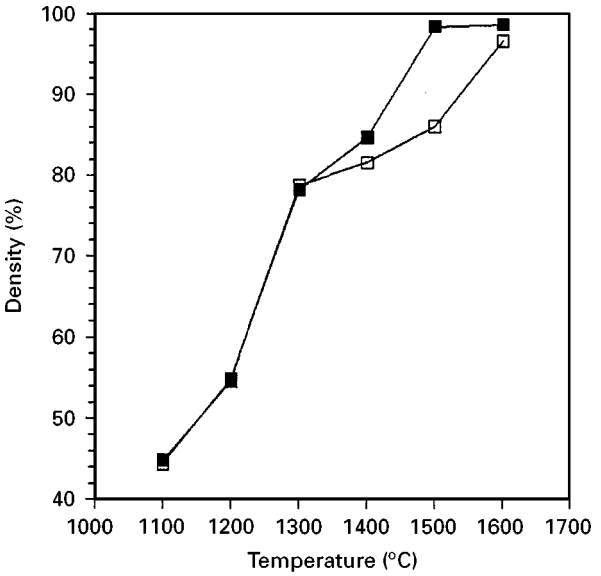

Figure 1 Relative density (% theoretical density) of (■) seeded and (□) unseeded alumina–mullite–zirconia (AMZ) composites sintered at various temperatures for 1 h.

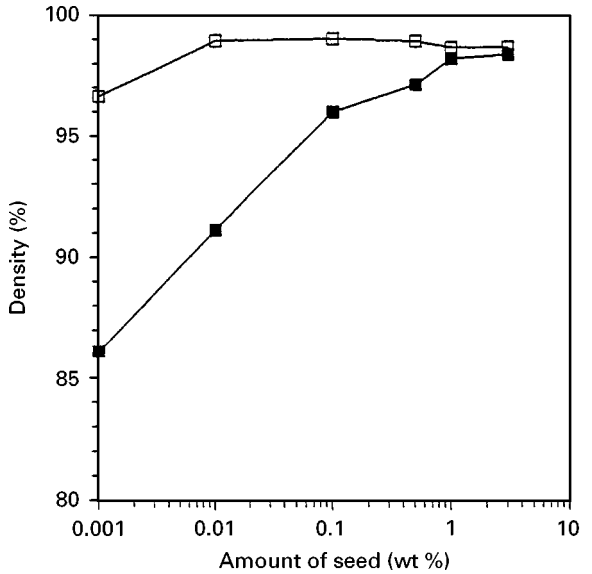

Figure 2 Relative density (% theoretical density) of alumina–mullite–zirconia composites plotted as a function of the amount of α-Al_2O_3 seeds. The composites were sintered either at (■) 1500 or (□) 1600 °C for 1 h.

seeding does not affect the sintered density below 1300 °C. However, for temperatures above 1300 °C, the increase in the sintered density is more pronounced in the 3 wt % α-Al_2O_3 seeded specimen. The seeded specimen sintered at 1500 °C for 1 h attains 98% of the theoretical density, ρ_{th}.

Fig. 2 shows the effect of the amount of α-Al_2O_3 seeding on the densification of AMZ composites sintered at two different temperatures for 1 h. For the composite specimens sintered at 1500 °C, the relative density increases constantly with increasing amount of α-Al_2O_3 seeding. On the other hand, the relative density of the composites sintered at 1600 °C is approximately 99% ρ_{th} and is essentially independent of the amount of seeds. Therefore, both the results of Figs 1 and 2 indicate that the α-Al_2O_3 seeding facilitates the densification of AMZ composites for temperatures between 1300 and 1500 °C.

The linear shrinkage of both α-Al_2O_3 seeded and unseeded specimens was examined as a function of temperature (Fig. 3). All the composite specimens were heated to a desired temperature at a heating rate of 5 °C min^{-1} and immediately quenched to room temperature without holding. Fig. 3 clearly shows that the densification of both α-Al_2O_3 seeded and unseeded specimens is characterized by three distinct stages. Stage I is represented by a rapid shrinkage between 1100 and 1300 °C. On the other hand, the densification is temporarily ceased at Stage II. A restoration of the shrinkage is evident at Stage III for temperatures above 1450 °C. Examination of the BET surface area of the powder compacts as a function of temperature indicated that the densification at Stage I was accompanied with a rapid reduction of the surface area, from 103 $m^2 g^{-1}$ at 1100 °C to 15 $m^2 g^{-1}$ at 1300 °C. On the other hand, the densification at Stage III is concomitant with a much smaller change in the surface area, from 7 $m^2 g^{-1}$ at 1450 °C to 3 $m^2 g^{-1}$ at 1500 °C. This result suggests that the observed rapid shrinkage in the lower temperature region, i.e. stage I, is caused by a viscous-flow sintering.

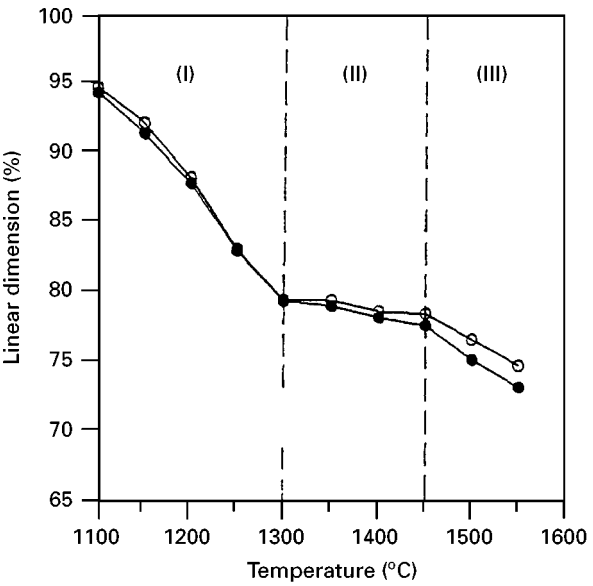

Figure 3 Linear shrinkage curves of (●) seeded and (○) unseeded alumina–mullite–zirconia composites plotted as a function of temperature. All the specimens were heated to the desired temperature at a heating rate of 5 °C min^{-1} and then quenched to room temperature without holding.

The origin of the three characteristic stages observed in the densification of AMZ composites can be comprehensively understood by examining the phase-formation characteristics of the precursor powder compacts discussed in a previous paper [1]. Fig. 4 shows the relative XRD peak intensities of the (1 1 3) plane of α-Al_2O_3 ($2\theta = 43.36°$) and the (2 1 0) plane of mullite ($2\theta = 26.27°$) plotted as a function of temperature. The data shown in Fig. 4 were taken from the specimens heated to a desired temperature and cooled immediately without holding. For both the seeded and unseeded specimens, the onset of mullitization is approximately 1300 °C. In addition, the crystalline form of SiO_2 was not observed in the boehmite–silica–

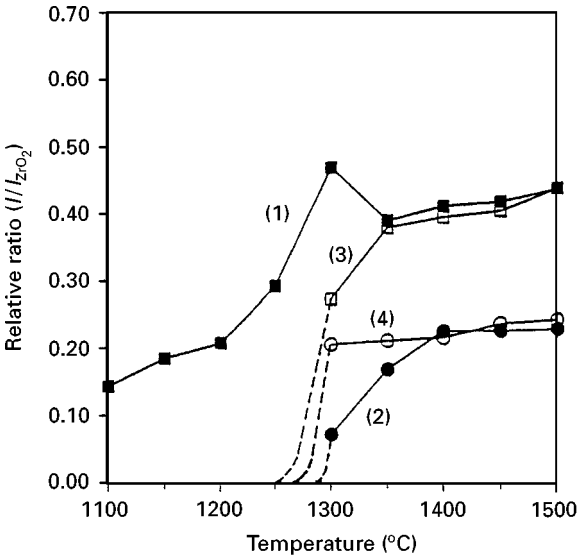

Figure 4 Relative XRD peak intensities (1, 3) of the (1 1 3) plane of α-Al_2O_3 and (2, 4) the (2 1 0) plane of mullite plotted as a function of temperature. The total intensity for zirconia was taken as an internal standard. The specimens were heated to the desired temperature and cooled immediately without holding. (1, 2) Seeded, (3, 4) unseeded.

zirconia pellets for the whole temperature range between 500 and 1600 °C [1]. Therefore, silica remains amorphous below 1300 °C. Amorphous silica usually undergoes a rapid densification by a viscous-flow sintering below 1300 °C, and this phenomenon was successfully applied to the fabrication of ceramic composites containing an SiO_2 component [3]. All these facts clearly indicate that the observed rapid shrinkage at Stage I is caused by the viscous-flow sintering of SiO_2 component in the boehmite–silica–zirconia powder compact before the onset of crystallization to mullite.

The observed plateau at Stage II is a direct consequence of the mullitization. As shown in Fig. 4, the mullitization is initiated at ~1300 °C. The formation of mullite ($3Al_2O_3{\cdot}2SiO_2$) then leads to the exhaustion of amorphous SiO_2 in the precursor powder, thereby inhibiting further densification above 1300 °C. Therefore, the observed plateau behaviour at Stage II is caused by the crystallization of the amorphous SiO_2 component. It was shown that the crystallization in the boehmite–silica–zirconia powder compact completed at ~1400 °C [1]. Therefore, a further densification observed above 1450 °C (Stage III; Fig. 3) is related to a solid-state diffusion sintering after the crystallization processes are completed.

The effect of α-Al_2O_3 seeding on the densification is apparent at Stages II and III. As shown in Fig. 4, the α-Al_2O_3 seeding retards the rate of mullite formation. This reduces the rate of silica consumption above 1300 °C. Therefore, the observed enhanced densification of the seeded specimens at Stage II is caused by the continuation of the viscous-flow sintering of the remnant silica component. On the other hand, the mullitization in the unseeded specimens occurs rapidly and is essentially completed at 1300 °C (Fig. 4), eliminating further possibility of viscous sintering.

3.2. Microstructural development

The pore-size distribution was first examined to monitor the microstructural evolution of the AMZ composites during the early and intermediate stages of sintering (for $\rho < 92\%\ \rho_{th}$). Fig. 5 shows the incremental pore-size distribution of the unseeded composite specimens sintered at various indicated temperatures for 1 h. The specimen sintered at 1600 °C was in the closed pore (final) stage and, thus, could not be used in a mercury-intrusion experiment. Although the porosity decreases significantly with increasing sintering temperature, the most frequent pore diameter (pore size at the maximum pore-size distribution; MFPD) increases slightly as temperature increases. This type of pore coarsening at the beginning of densification is frequently observed [4–6]. The seeded composite specimens also exhibited the same type of pore-size evolution during the early and intermediate stages of densification.

Fig. 6 shows scanning electron micrographs of the AMZ composites (50 wt % alumina–30 wt % mullite–20 wt % zirconia) sintered either at 1500 or at 1600 °C for 1 h. As shown in the micrographs, the spatial distribution of zirconia particles is uniform and is not affected by the α-Al_2O_3 seeding. The unseeded specimen sintered at 1500 °C shows large pores with $\rho = \sim 86\%\ \rho_{th}$. On the other hand, the α-Al_2O_3 seeded specimen sintered at the same conditions shows an essentially pore-free microstructure ($\rho = \sim 99\%\ \rho_{th}$; Fig. 6b) and is characterized by small-sized grains (~0.4 μm). For the sintering at 1600 °C, the most outstanding microstructural difference between the α-Al_2O_3 seeded specimen and the unseeded specimen is the shape of the matrix grains. As shown in Fig. 6c, the unseeded specimen shows equiaxed matrix grains on the whole. On the contrary, the α-Al_2O_3 seeded specimen is more or less characterized by elongated grains.

The effects of the amount of α-Al_2O_3 seeds on the sintered microstructure are shown in Fig. 7. For the

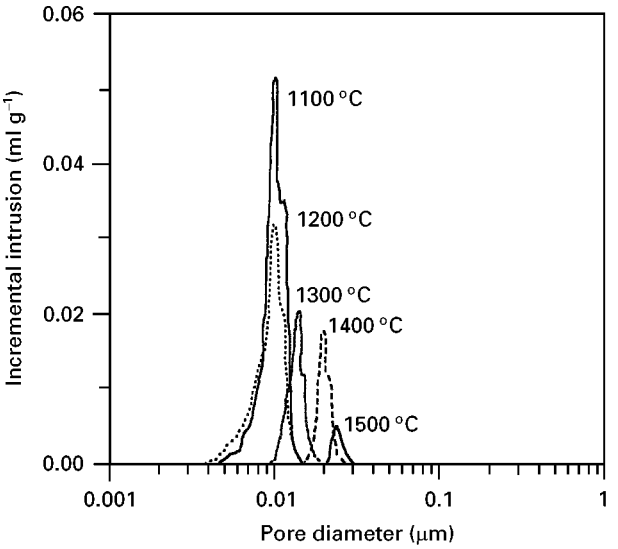

Figure 5 Incremental pore-size distribution of unseeded alumina–mullite–zirconia composite specimens sintered at various temperatures for 1 h.

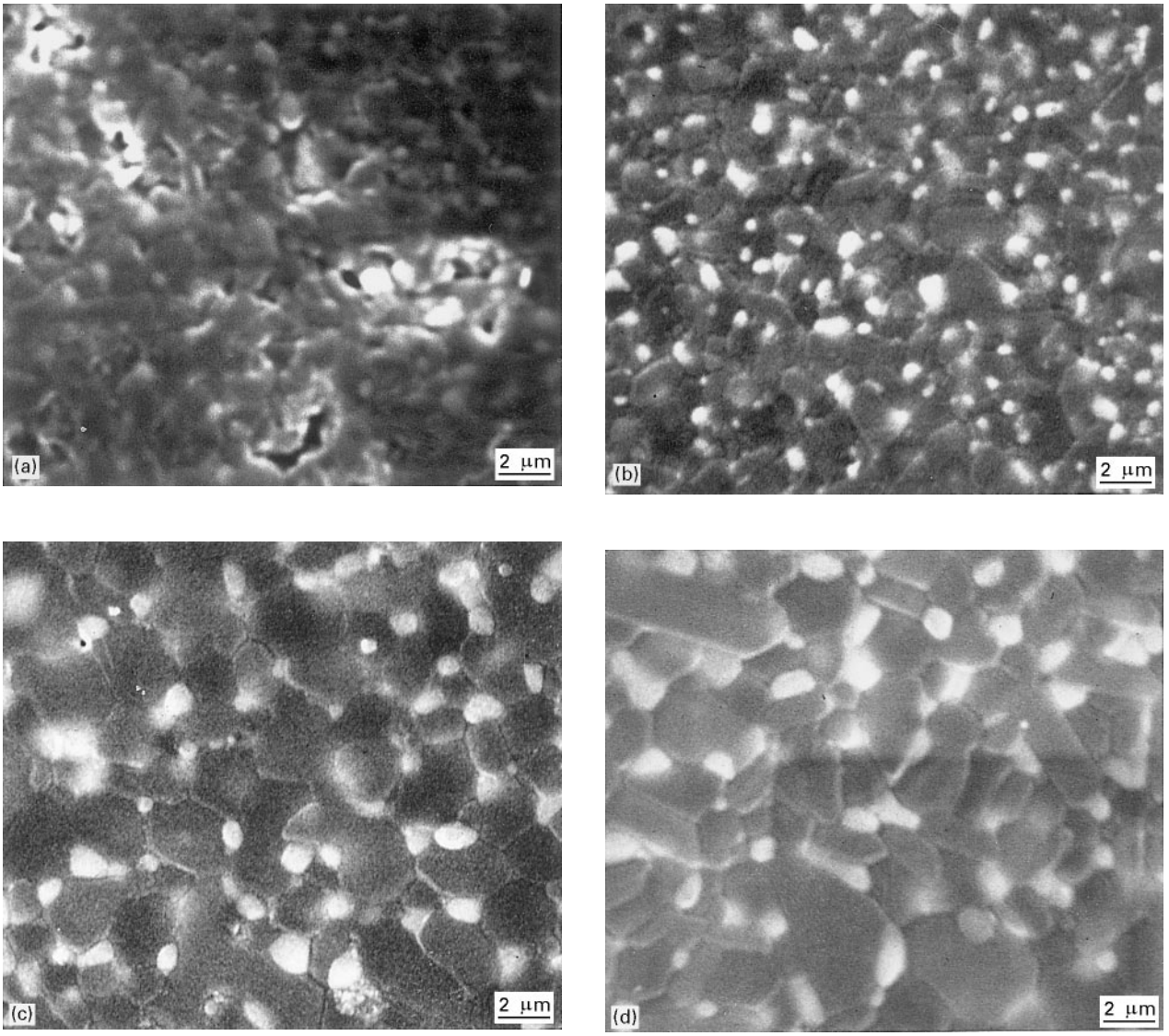

Figure 6 Scanning electron micrographs of alumina–mullite–zirconia composites sintered either at 1500 or at 1600 °C for 1 h: (a) unseeded specimen sintered at 1500 °C for 1 h; (b) 3 wt % α-Al_2O_3 seeded specimen sintered at 1500 °C for 1 h; (c) unseeded specimen sintered at 1600 °C for 1 h; (d) 3 wt % α-Al_2O_3 seeded specimen sintered at 1600 °C for 1 h.

specimens sintered at 1600 °C for 1 h, both the density (Fig. 2) and the average grain size (Fig. 7) are not significantly affected by the amount of α-Al_2O_3 seeds added to the composites. However, the shape of matrix grains gradually becomes elongated as the amount of α-Al_2O_3 seeds increases. This microstructural feature was also preserved in the composite specimens sintered for longer times. As shown in Fig. 8, the α-Al_2O_3 seeding significantly influences the shape of grains in the composite specimens sintered at 1600 °C for 24 h. All these results (Figs 6, 7 and 8) indicate that the α-Al_2O_3 seeding induces the formation of elongated grains in the AMZ composites.

Figs 9 and 10 show the results of EPMA analysis for the 3 wt% α-Al_2O_3 seeded composite specimens sintered at 1600 °C for 24 h. The result of elemental silicon-mapping is shown in Fig. 9a, and the white spots indicate the presence of silicon atoms. The micrograph in Fig. 9b shows the sintered microstructure of the corresponding region. A careful examination of Figs 9a and b indicates that the elongated grains are relatively deficient in silicon content. A more quantitative information on the distribution of constitutive atoms (Si, Al) was obtained by examining the result of EPMA point analysis (Fig. 10). Region A represents a typical elongated grain, and the corresponding EPMA spectrum indicates that the ratio of aluminium to silicon is approximately 50. Contrary to this, the ratio of aluminium to silicon in a typical equiaxed grain (Region B) is approximately 5. Therefore, the equiaxed grains mainly correspond to mullite, while the elongated grains largely constitute corundum (α-Al_2O_3) phase.

From the results shown in Figs 6–10, one can conclude that the α-Al_2O_3 seeding facilitates the formation of elongated grains, and these elongated grains correspond to α-Al_2O_3. The anisotropic grain growth of alumina is a well known phenomenon. However, the mechanism of this anisotropic growth is not clearly understood, despite extensive studies on this subject [7–10]. It is generally believed that the presence of CaO or SiO_2 above a certain critical concentration, facilitates the anisotropic grain growth and faceting of alumina [8–10]. In view of this, the

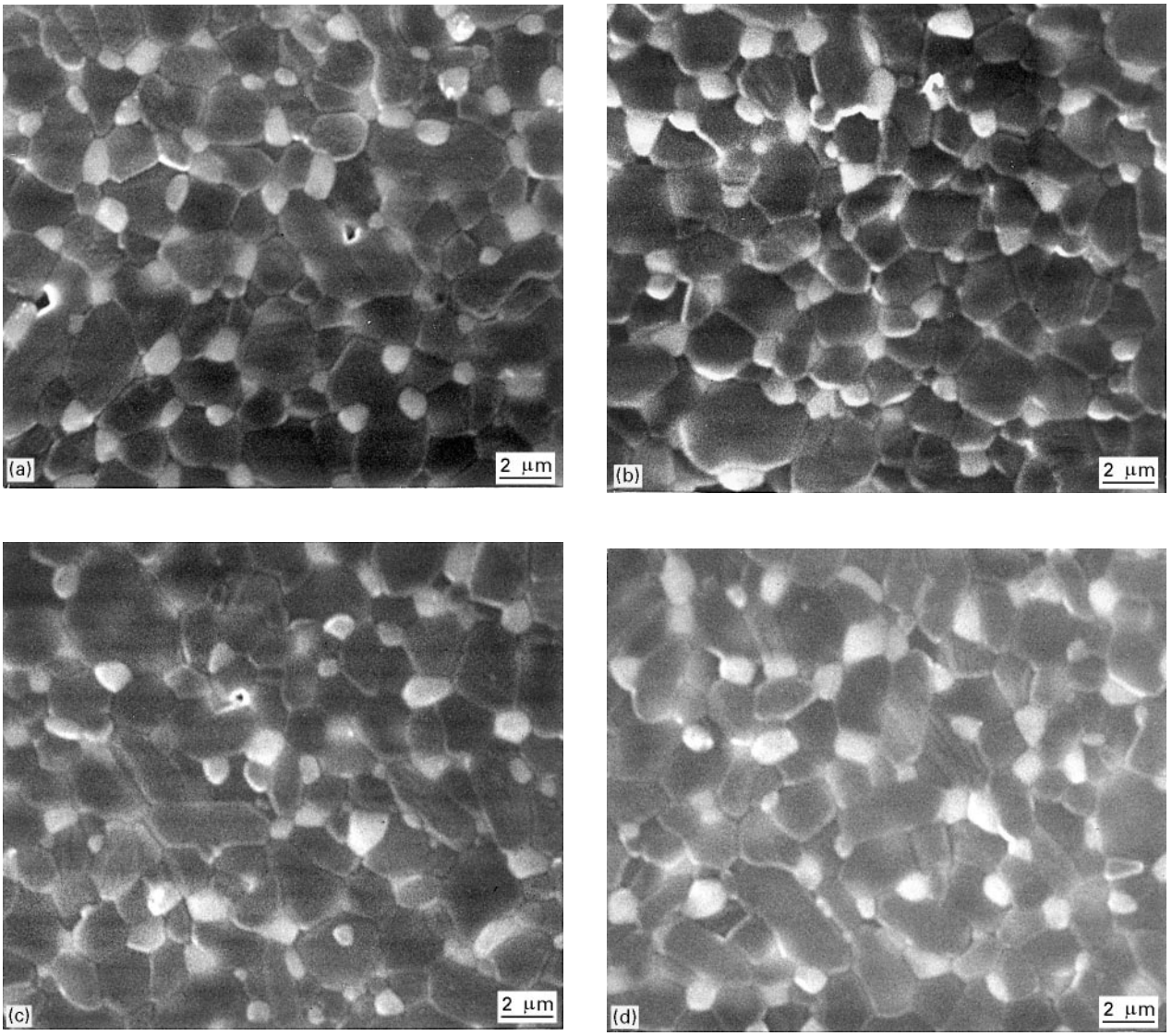

Figure 7 Scanning electron micrographs of alumina–mullite–zirconia composites containing various amounts of α-Al_2O_3 seeds. All the specimens were sintered at 1600 °C for 1 h: (a) 0.01 wt % α-Al_2O_3 seeded specimen; (b) 0.1 wt % α-Al_2O_3 seeded specimen; (c) 0.5 wt % α-Al_2O_3 seeded specimen; (d) 1 wt % α-Al_2O_3 seeded specimen.

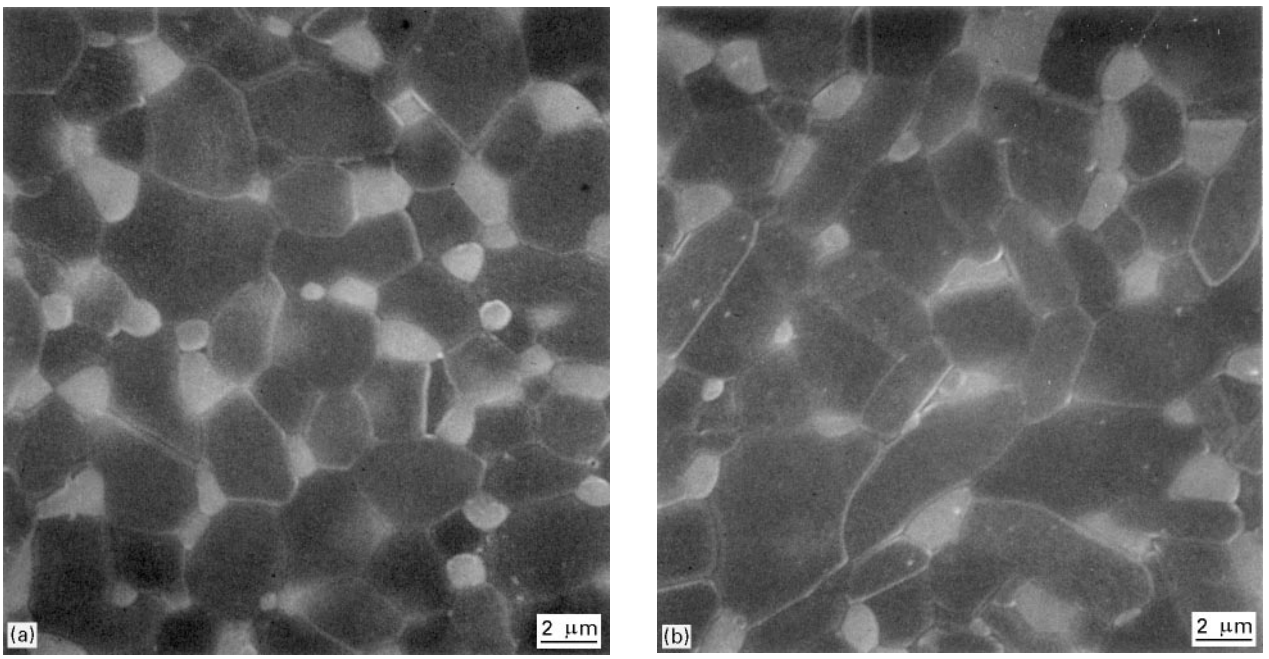

Figure 8 Scanning electron micrographs of polished surfaces of alumina–mullite–zirconia composites sintered at 1600 °C for 24 h: (a) unseeded specimen, (b) 3 wt % α-Al_2O_3 seeded specimen.

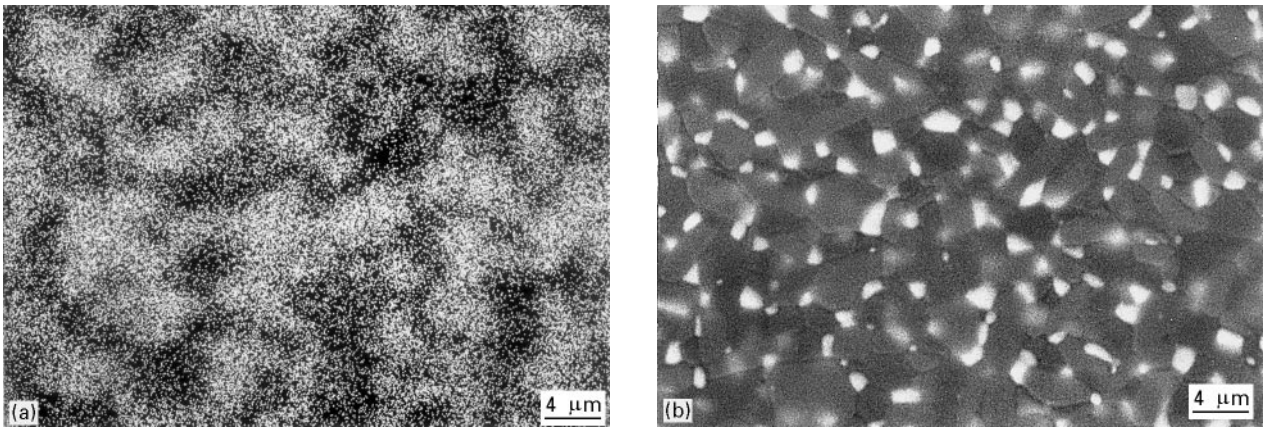

Figure 9 Elemental mapping of silicon atoms for 3 wt% α-Al_2O_3 seeded composite specimen sintered at 1600 °C for 24 h. The white spots in (a) represent the location of silicon atoms; (b) shows the corresponding microstructure.

observed anisotropic grain growth of alumina in the α-Al_2O_3 seeded AMZ composites is closely related to the presence of SiO_2 component in the alumina–silica–zirconia precursor powder.

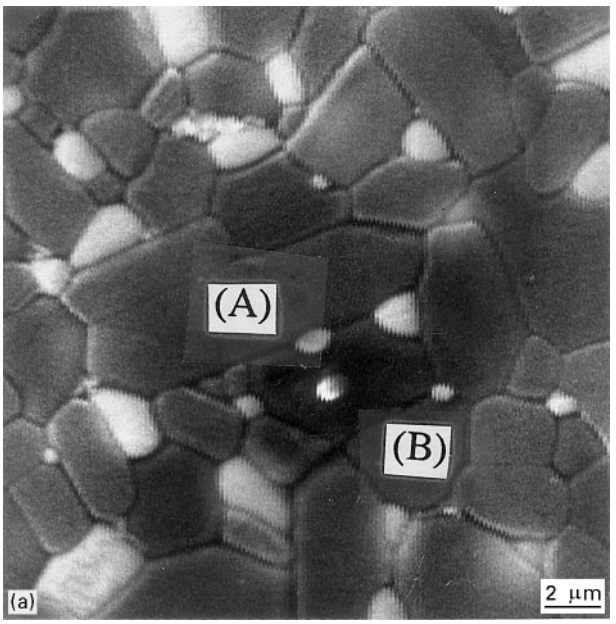

Since the anisotropic grain growth was not observed in the unseeded specimens, the change in the mechanism of phase formation by the α-Al_2O_3 seeding must be closely related to the anisotropic grain growth in the AMZ composites. As shown in Fig. 4, the relative fractions of both α-Al_2O_3 and mullite in the unseeded specimens increase rapidly above 1250 °C. On the other hand, the peak intensity corresponding to α-Al_2O_3 increases gradually in the seeded specimen, while the formation of mullite is retarded by the α-Al_2O_3 seeding. Therefore, the delayed mullitization in the seeded specimen leaves the amorphous silica unconsumed up to 1250 °C. It is quite possible that this unreacted amorphous silica is incorporated into the epitaxially growing α-Al_2O_3 around the α-Al_2O_3 seeds. On the other hand, both α-Al_2O_3 and mullite form simultaneously above a certain critical temperature ($\sim$1250 °C) in the unseeded specimen, excluding the possibility of incorporating the SiO_2 component in the growing α-Al_2O_3 particles. Therefore, one can draw the following conclusions on the effects of α-Al_2O_3 seeding on the observed anisotropic grain growth: the α-Al_2O_3 seeding selectively induces the epitaxial growth of α-Al_2O_3 before mullitization begins. The unreacted SiO_2 component in the

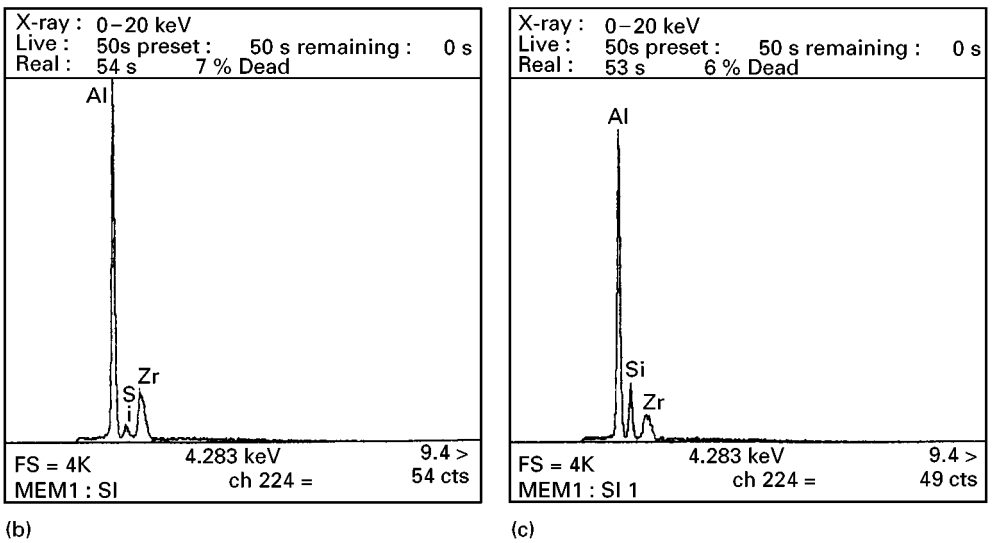

Figure 10 (a) Scanning electron micrograph, and (b, c) EPMA spectra of two selected regions (A, B, respectively) in 3 wt% α-Al_2O_3 seeded composite specimen sintered at 1600 °C for 24 h.

precursor is incorporated into the growing α-Al_2O_3 particles until the mullitization begins near 1300 °C, facilitating the anisotropic grain growth of α-Al_2O_3.

3.3. Fracture toughness

The relative fraction of tetragonal zirconia as a function of the total zirconia content was estimated [11] to examine the roles of tetragonal phase in the toughening of alumina–mullite–zirconia composites. As shown in Fig. 11, the tetragonal fraction in the ground surface is smaller than that in the as-sintered surface for the whole range of total zirconia content in the composites, indicating the presence of the transformed zirconia particles caused by the grinding after sintering. This result suggests that the tetragonal → monoclinic (t → m) transformation toughening potentially contributes to the toughening of AMZ composites. Fig. 11 also shows that the tetragonal fraction decreases with increasing zirconia content. This can be explained in terms of the coarsening of zirconia particles. Increasing the content of zirconia expedites the particle coalescence and coarsening, thereby decreasing the stability of tetragonal phase near room temperature. Therefore, the relative contribution of the t → m transformation toughening is expected to be decreased rapidly with increasing zirconia content.

Fracture toughness data of the AMZ composite specimens are presented in Fig. 12 as a function of the total zirconia content. For the purpose of K_{1c} measurements, the weight ratio of alumina to mullite in the composites was kept at a fixed value of 5: 3, and the total zirconia content was varied from 0–40 wt %. K_{1c} increases from 2.25 MPa $m^{1/2}$ for the 50 wt % alumina–30 wt % mullite composite, to 5.25 MPa $m^{1/2}$ for the polished and annealed composite containing 40 wt % zirconia. Because the monoclinic zirconia particles formed during the mechanical polishing transform back to the tetragonal state upon annealing, K_{1c} of the polished and annealed composite is expected to be greater than K_{1c} of the unannealed composite for a given zirconia content. However, as shown in Fig. 12, the increase in K_{1c} upon annealing at 1300 °C for 1 h is not pronounced for a wide range of zirconia content. This presumably suggests that the transformation zone introduced by polishing (machining) is not thick enough to contribute significantly to the decrease in K_{1c}. Another possible explanation of this observation is that the toughening effect caused by the monoclinic phase is comparable to that of the t → m transformation.

As shown in Fig. 12, the fracture toughness is approximately linearly proportional to the total zirconia content in the composites. Fig. 11 indicates that the relative fraction of monoclinic phase increases rapidly with increasing zirconia content. Because the most important toughening mechanism caused by the monoclinic phase is the microcrack nucleation [12–14], these results indicate that the toughening by the microcrack nucleation becomes increasingly important as the total content of zirconia increases.

According to the model of transformation toughening proposed by McMeeking and Evans [15], the

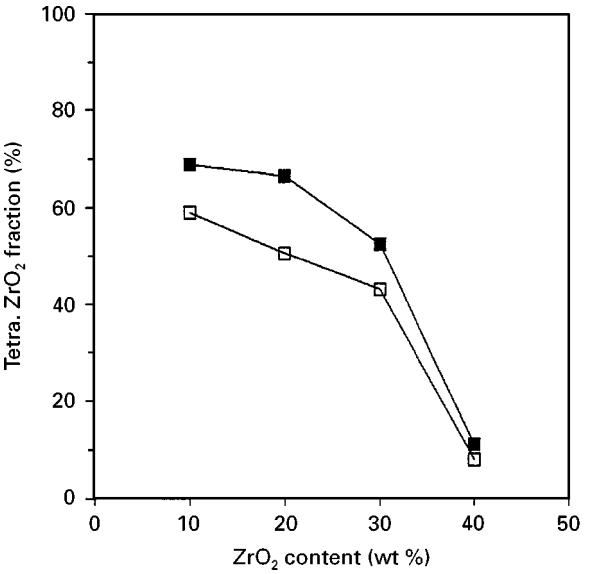

Figure 11 Fraction of tetragonal zirconia plotted as a function of total content of zirconia in alumina–mullite–zirconia composites: (■) as-sintered, (□) after grinding. The weight ratio of alumina to mullite in the composites was kept at a fixed value of 5:3. All the specimens were sintered at 1600 °C for 1 h.

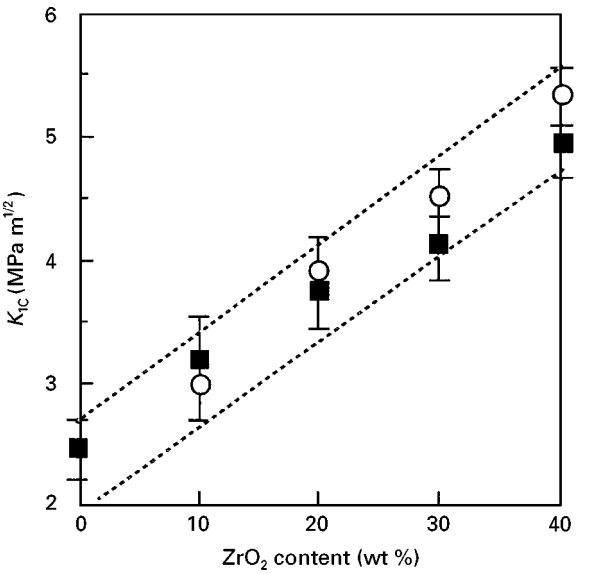

Figure 12 Fracture toughness values of alumina–mullite–zirconia composites plotted as a function of zirconia content. All the composite specimens were sintered at 1600 °C for 1 h and polished. Parts of the sintered specimens were subsequently annealed at 1300 °C for 1 h. (■) Polished, (○) polished and annealed.

increment of fracture toughness caused by the transformation toughening is proportional to the volume fraction of tetragonal zirconia particles. Their analysis is based on the reduction in crack-tip stress intensity provided by the transformation-induced stresses. Considering the energy dissipation associated with the transformation toughening, Chen [16] also obtained essentially the same result. The extent of the transformation toughening for both models can be represented by the following equation

$$\Delta K_T = ae^T E V_{f(t)} h^{1/2}/(1-\nu) = C V_{f(t)} \qquad (1)$$

where e^T is the strain caused by the transformation, E is the Young's modulus of the matrix, ν is Poisson's

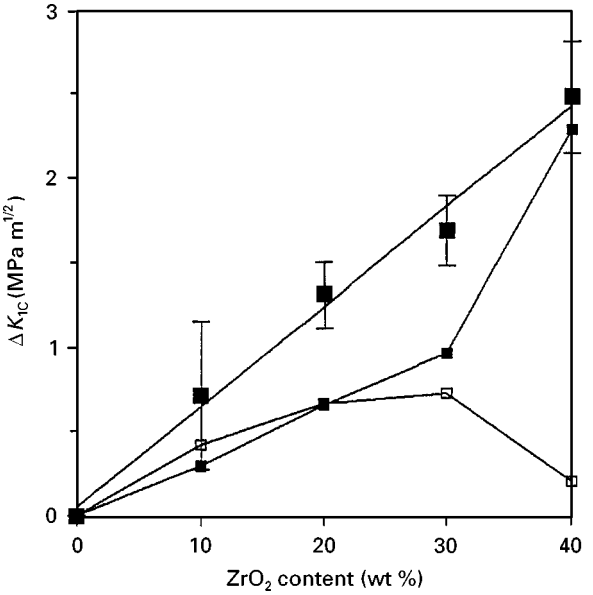

Figure 13 Relative contributions of (□) the transformation toughening, ΔK_T, and (■) the microcrack nucleation, ΔK_M, to (■) the net increment in fracture toughness, ΔK_{1c}, of alumina–mullite–zirconia composites sintered at 1600 °C for 1 h.

ratio, h is the width of the transformation zone, $V_{f(t)}$ is the volume fraction of tetragonal particles, and a is a numerical constant (0.22 for the McMeeking–Evans model, and 0.4783 for Chen's model).

Fig. 12 shows that the fracture toughness of the AMZ composites is proportional to the total content of zirconia and is independent of the relative fraction of tetragonal and monoclinic phases. Therefore, the net toughening effect caused by the presence of zirconia particles (ΔK) can be empirically written as

$$\Delta K = C' V_{f(ZrO_2)} = C'(V_{f(t)} + V_{f(m)}) = \Delta K_T + \Delta K_M \quad (2)$$

where C' is another proportionality constant, $V_{f(ZrO_2)}$ is the volume fraction of total zirconia particles (tetragonal + monoclinic) in a composite, $V_{f(m)}$ is the volume fraction of monoclinic particles, and ΔK_M is the toughening increment caused by the monoclinic particles. The last equality in Equation 2 is based on the assumption that both the t → m transformation toughening and the toughening by the monoclinic zirconia independently (separately) contribute to the fracture toughness. Comparing the above empirical relation with Equation 1 then predicts that $C = C'$. This implies that the toughening caused by the monoclinic particles, and thus by the microcrack nucleation, is comparable to that by the t → m martensitic transformation [14]. The toughening increments via these two distinct mechanisms can now be separately estimated using the above discussion (Equation 2) and the results shown in Figs 11 and 12. As shown in Fig. 13, the toughening enhancement caused by the microcrack nucleation, ΔK_M, increases as the total content of zirconia increases. This reflects that the fraction of monoclinic phase increases with increasing zirconia content (Fig. 11).

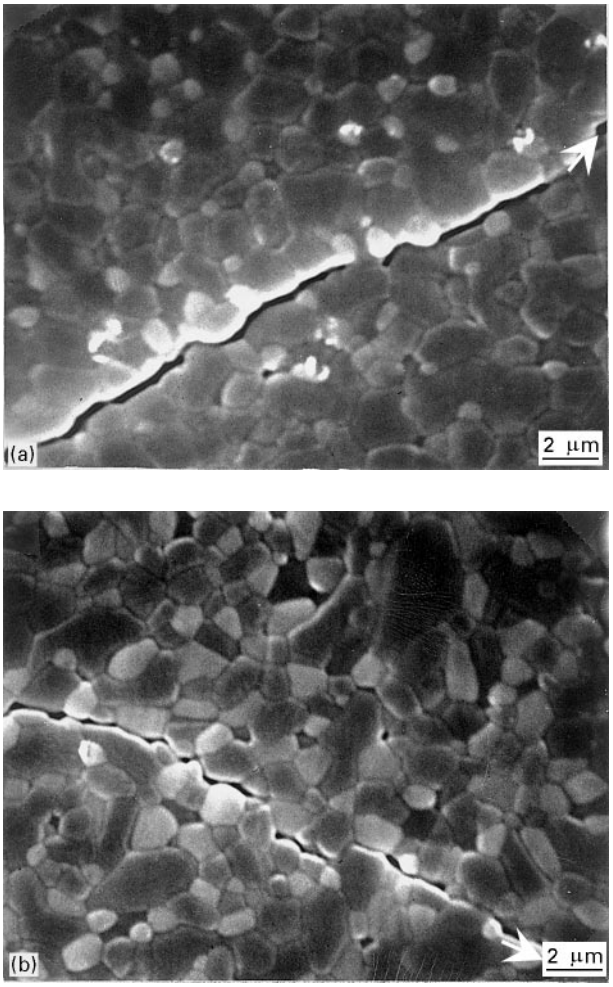

Figure 14 Scanning electron micrographs of indented alumina–mullite–zirconia composites sintered at 1600 °C for 1 h. The arrows indicate the directions of crack propagation: (a) composite specimen containing 20 wt % zirconia; (b) composite specimen containing 40 wt % zirconia.

Fig. 13 shows that the toughening increment at 40 wt % ZrO_2 is mainly caused by the monoclinic particles. This suggests that some toughening mechanism other than the microcrack nucleation/transformation toughening presumably contributes to the increased toughness. A crack deflection mechanism seems to contribute somewhat to the increase in toughening, because it provides toughening regardless of temperature and particle size [17]. Because the thermal expansion coefficient of zirconia is significantly larger than that of the alumina–mullite matrix, cooling from processing puts the zirconia particles in tension and the matrix in hoop compression. Therefore, the crack is not attracted to the dispersed zirconia particles but should deflect around them. Fig. 14 shows typical features of crack propagation in the indented AMZ composites containing 20 and 40 wt % zirconia. A crack propagates straight into the matrix region but deflects around the dispersed zirconia particles.

4. Conclusions

Densification characteristics and fracture toughness of the alumina–mullite–zirconia (AMZ) composites

prepared by the colloidal processing route were systematically examined. The following conclusions were drawn.

1. The densification of boehmite–silica–zirconia precursor compacts was characterized by three distinct stages. Stage I was represented by a rapid shrinkage between 1100 and 1300 °C and was caused by the viscous flow sintering of the SiO_2 component. Stage II was characterized by a temporary cessation of the linear shrinkage and was a direct consequence of the mullitization. Stage III was represented by a restoration of the shrinkage for temperatures above 1450 °C and was related to a solid-state diffusion sintering after the crystallization processes were completed.

2. The α-Al_2O_3 seeding facilitated the formation of elongated grains in the AMZ composites, and these elongated grains correspond to α-Al_2O_3.

3. The toughening caused by the microcrack nucleation was comparable to that by the t $\rightarrow$ m martensitic transformation and increased as the total content of zirconia in the AMZ composite increased.

References

1. H. M. JANG, S. M. CHO and K. T. KIM, *J. Mater. Sci.* (1996) in press.
2. B. R. LAWN and E. R. FULLER, *ibid.* **10** (1975) 2016.
3. M. D. SACKS, N. BOZKURT and G. W. SCHEIFFELE, *J. Am. Ceram. Soc.* **74** (1991) 2428.
4. F. F. LANGE, *ibid.* **67** (1984) 83.
5. T. KIMURA, Y. MATSUDA, M. ODA, and T. YAMAGUCHI, *Ceram. Int.* **13** (1987) 27.
6. J. ZHENG and J. S. REED, *J. Am. Ceram. Soc.* **72** (1989) 810.
7. W. A. KAYSSER, M. SPRISSLER, C. A. HANDWERKER, and J. E. BLENDELL, *ibid.* **70** (1987) 339.
8. C. A. HANDWERKER, P. A. MORRIS and R. L. COBLE, *ibid.* **72** (1989) 130.
9. H. SONG and R. L. COBLE, *ibid.* **73** (1990) 2086.
10. Y. K. SIMPSON and C. B. CARTER, *ibid.* **73** (1990) 2391.
11. R. C. GARVIE and P. S. NICHOLSON, *ibid.* **55** (1972) 303.
12. K. T. FABER, *Ceram. Eng. Sci. Proc.* **5–6** (1984) 408.
13. A. G. EVANS and K. T. FABER, *J. Am. Ceram. Soc.* **67** (1984) 255.
14. M. RÜHLE, N. CLAUSSEN and A. H. HEUER, *ibid.* **69** (1986) 195.
15. R. M. McMEEKING and A.G. EVANS, *ibid.* **65** (1982) 242.
16. I. W. CHEN, *ibid.* **74** (1991) 2564.
17. A. G. EVANS, in "Advances in Ceramics", Vol. 12, "Science and Technology of Zirconia II", edited by N. Claussen, M. Rühle and A. H. Heuer (American Ceramic Society, Columbus, OH, 1984) p. 193.

Received 2 October 1995
and accepted 18 March 1996